



Electrochemical synthesis and characterization of basic bismuth nitrate $[\text{Bi}_6\text{O}_5(\text{OH})_3](\text{NO}_3)_5 \cdot 2\text{H}_2\text{O}$: a potential highly efficient sorbent for textile reactive dye removal

Slobodan M. Najdanović¹ · Milica M. Petrović¹ · Miloš M. Kostić¹ · Jelena Z. Mitrović¹ · Danijela V. Bojić¹ · Milan D. Antonijević² · Aleksandar Lj. Bojić¹

Received: 2 June 2019 / Accepted: 13 September 2019 / Published online: 23 September 2019
© Springer Nature B.V. 2019

Abstract

A new method of synthesis was developed for the preparation of basic bismuth nitrate $[\text{Bi}_6\text{O}_5(\text{OH})_3](\text{NO}_3)_5 \cdot 2\text{H}_2\text{O}$ (ECBBN). Electrochemical synthesis of the material was carried out by galvanostatic electrodeposition from an acidic Bi(III) solution on a Ti substrate and further thermal treatment in air at 200 °C. Characterization of ECBBN was conducted by employing SEM–EDX, N_2 adsorption, XRD and FTIR, and its pI was also determined. The analyses showed that the material obtained was pure $[\text{Bi}_6\text{O}_5(\text{OH})_3](\text{NO}_3)_5 \cdot 2\text{H}_2\text{O}$. Morphologically, ECBBN aggregates were composed of crystals, some smaller than 50 nm. Electrochemically synthesized sorbent (ECBBN) was used for the removal of the textile dye Reactive Blue 19 (RB19) from deionized water and model solutions of polluted river water, and it showed considerably superior sorption performance compared to other inorganic sorbents synthesized by conventional methods reported in the literature. A kinetic study suggests that the sorption process is both under reaction and diffusion control. Equilibration of the sorption process was attained in several minutes, i.e. the sorption process is very fast. The sorption equilibrium data were well interpreted by the Langmuir, Redlich–Peterson and Brouers–Sotolongo isotherm. Using Langmuir isotherm, the maximum sorption capacity of ECBBN was reached at pH 2 and was 1049.19 mg g^{-1} .

Keywords Basic bismuth nitrate · Electrochemical synthesis · Sorption · Textile dye · Reactive Blue 19

✉ Slobodan M. Najdanović
najda89@gmail.com

¹ Department of Chemistry, Faculty of Sciences and Mathematics, University of Niš, Višegradska 33, 18000 Niš, Serbia

² Faculty of Engineering and Science, University of Greenwich at Medway, Central Avenue, Chatham Maritime, Kent ME4 4TB, England, UK

Abbreviations

BBN	Basic bismuth nitrate
ECBBN	Electrochemically synthesized $[\text{Bi}_6\text{O}_5(\text{OH})_3](\text{NO}_3)_5 \cdot 2\text{H}_2\text{O}$
RB19	Reactive Blue 19
pI	Isoelectric point

Introduction

Synthetic dyes are major industrial pollutants and water contaminants due to their large-scale production and extensive applications [1]. Many industries, such as dye, textile, cosmetic, paper, plastics, leather, rubber, food and pharmaceuticals use dyes to colour their products [2–4]. Significant quantities of synthetic dyes are discharged into the environment from industrial effluents [5]. They give an intense colour to the water and are toxic to the aquatic environment. Hence, wastewater from dye production and industrial applications presents a serious threat to the environment [6, 7]. Reactive Blue 19 (RB19) is an anthraquinone dye, and because it is highly stabilized by resonance, it is very resistant to chemical oxidation [8]. Several techniques such as chemical oxidation, biodegradation, photodegradation, electrocoagulation, membrane separation and reverse osmosis have been developed for treating water pollutants [9–13]. There are many studies of photocatalytic degradation of RB19 by different bismuth compounds used as photocatalyst [14–19]. Relative to the foregoing techniques adsorption is considered to be simple, highly efficient and relatively inexpensive, and in a lot of studies, various organic and inorganic compounds are successfully used for removal of RB19 dye [9, 20–27].

Basic bismuth nitrates (BBNs) in recent works are used as photocatalysts [28–30] and in rare cases as sorbents [31] for pollutants removal from water. They are also used in medicine for the treatment of gastric and duodenal ulcers, gastritis, dyspepsia, inflamed skin and functional disorders of the large intestine, stomach and duodenum [32]. Typical synthetic methods for the preparation of BBNs include precipitation [31], hydrolysis [30], hydrothermal [28] and microwave-assisted hydrothermal methods [29].

Electrodeposition, as one of the most common methods of electrochemical synthesis, is very attractive for material synthesis due to its simplicity and ability to easily control of deposition rate, thickness and uniformity of deposit by changing of the electrodeposition process parameters [33]. To our knowledge, electrochemical synthesis of BBNs has not been reported in the scientific literature.

The aim of the study reported herein was to develop a new method for the synthesis (electrochemical) of basic bismuth nitrate (ECBBN) and to characterize the product by scanning electron microscopy/energy-dispersive X-ray spectroscopy (SEM–EDX), nitrogen sorptometry, X-ray diffraction (XRD) and Fourier transform infrared spectroscopy (FTIR) analysis. In addition, the isoelectric point (pI) of the ECBBN was determined. In order to investigate its applicability for textile dye removal, removal of RB19 as a model pollutant in aqueous solutions was evaluated, as well as the removal of RB19 from model solutions of polluted river water. The influence of pH, sorbent dose and initial dye concentration was also examined.

Reaction and diffusion kinetics models (pseudo-first-order, pseudo-second-order and intraparticle diffusion), as well as isotherm models (Langmuir, Freundlich, Redlich–Peterson and Brouers–Sotolongo) were examined for a better understanding of the sorption process.

Experimental methods

Materials

Bismuth (III) nitrate pentahydrate was purchased from Acros Organics (USA). Nitric acid, sodium hydroxide, ethanol and RB19 were purchased from Sigma-Aldrich (Germany). All chemicals used in this study were of analytical grade and used without any further purification. Deionized water was used in all experiments.

Synthesis of basic bismuth nitrate

Basic bismuth nitrate was synthesized by electrodeposition from acidic bismuth nitrate solution ($0.1 \text{ mol dm}^{-3} \text{ Bi}(\text{NO}_3)_3$ in $1.0 \text{ mol dm}^{-3} \text{ HNO}_3$). Electrodeposition was conducted in a galvanostatic regime at a current density of 150.0 mA cm^{-2} for 5.0 min at ambient temperature ($25.0 \pm 0.5 \text{ }^\circ\text{C}$). A conventional two-electrode cell was used for electrodeposition. A sheet of titanium ($10 \times 20 \text{ mm}$) was used as the working electrode (cathode), while stainless-steel sheet ($10 \times 20 \text{ mm}$) was used as the counter electrode (anode). The working and counter electrodes were at a distance of 15 cm. All the electrodes were cleaned before the electrodeposition by polishing with different abrasive papers and ultrasonic cleaning in ethanol and deionized water. Electrodeposition was carried out using an Amel 510 DC potentiostat (Materials Mates, Italy) and a VoltaScope software package. After electrodeposition, the titanium sheet with deposited material was dried at room temperature for 120 min. Finally, basic bismuth nitrate was obtained by thermal treatment at $200 \text{ }^\circ\text{C}$ for 90 min. After cooling in air, the synthesized material was removed from the titanium sheet and powdered.

Characterization of sorbent

For SEM–EDX analysis, samples were attached to aluminium stubs using Leit-C carbon cement. A cold FEG-SEM (SU8030, Hitachi, Japan) was used for imaging the samples with Noran NSS system 7 ultra-dry X-ray detector (Thermo-scientific, USA) for semi-quantitative EDX analysis. Samples were imaged uncoated. Nitrogen adsorption measurements were performed on a Gemini 5 Surface Area Analyser (Micromeritics, Norcross, Georgia, USA). Before the measurement, the samples were degassed under flowing nitrogen at $40 \text{ }^\circ\text{C}$ for 20 h. The specific surface area was determined using the Brunauer–Emmett–Teller (BET) method [34]. The Barret–Joyner–Halenda (BJH) method was used for pore volume, area and diameter analysis [35]. The crystal structure was identified by X-ray diffraction (XRD) using a powder X-ray

diffractometer (Ultima IV, Rigaku, Japan). XRD studies of all the powders were conducted using Cu K α radiation ($\lambda = 1.5406$ nm) produced at 40 kV and 40 mA. Experiments were performed in the scan range $2\theta = 5^\circ - 90^\circ$ under 40 kV, 40 mA, using a scan speed 5° min^{-1} and step size of 0.02° . Before the measurements, angular corrections were undertaken by using a reference Si standard. FTIR (Fourier transform infrared spectrometer) spectra were recorded using KBr discs in the range of $400 - 4000 \text{ cm}^{-1}$ using a BOMEM MB-100 (Hartmann & Braun, Canada) FTIR spectrometer. The number of scans was 16. The isoelectric point of the sorbent was determined by the salt addition method [36]. NaNO_3 solution (0.1 mol dm^{-3}) was used as an inert electrolyte and a series of test solutions were prepared by adjusting the pH of 50.0 cm^3 of electrolyte in the range 2.0–11.0 using 0.01 mol dm^{-3} HNO_3 and 0.01 mol dm^{-3} NaOH . Then 0.2 g of sorbent was added to each solution, sealed and stirred for 24 h, and the final pH (pH_f) was measured. The pH_i values were plotted against the initial pH (pH_i), and the pI was determined from the data where $\text{pH}_i = \text{pH}_f$.

Batch sorption experiments

Batch sorption experiments were performed to study the effect of parameters such as contact time, pH, sorbent dose and initial dye concentration, as well as to determine maximum sorption capacity. The experiments were carried out at ambient temperature in a Petri dish by adding the desired amount of sorbent in prepared solutions of RB19 and stirred using a magnetic stirrer, and a series of sorption experiments were done at different operating conditions by changing initial dye concentrations, initial sorbent doses, reaction times and pH of the solution. The pH of the experimental solutions was adjusted by adding HNO_3 or NaOH . Residual RB19 concentration was determined through the measurement of the dye solution absorbance at 592 nm by UV–visible spectrophotometer (UV-1800, Shimadzu, Japan). Before the measuring of absorbance, sorbent was separated from the solution by filtration using regenerated cellulose membrane filters with a $0.45 \mu\text{m}$ pore size (Agilent Technologies, Germany). The following equations were utilized for determining the sorbed amount of dye q_t (mg g^{-1}) and the dye removal efficiency (RE):

$$q_t = \frac{c_0 - c_t}{m} \cdot V \quad (1)$$

$$RE = \frac{c_0 - c_t}{c_0} \cdot 100\% \quad (2)$$

where c_0 and c_t (mg dm^{-3}) are the initial and final concentrations of the RB19, m (g) is the mass of the sorbent and V (dm^3) is the solution volume.

Relative mean deviation (RMD) was calculated by the following equation:

$$RMD = \frac{\sum_{i=1}^n |q_{i,\text{exp}} - q_{i,\text{cal}}|}{q_{\text{exp}} \cdot n} \cdot 100\% \quad (3)$$

where $q_{i, \text{exp}}$ (mg g^{-1}) is experimentally obtained amount of sorbed dye at the experimental point i , $q_{i, \text{cal}}$ (mg g^{-1}) is calculated amount of sorbed dye at the experimental point i by some kinetic or isotherm model and n is a number of the experimental points.

In order to find out whether there is any adsorption on the Petri dish walls, control experiments were carried out in the absence of sorbent, and it was concluded that sorption is negligible. The sorption experiments were conducted in triplicate. All calculations of the experimental data and statistical analysis were performed using OriginPro 2016 software (OriginLab Corporation, USA).

Results and discussion

Characterization of sorbent

SEM analysis

Figure 1 shows SEM images of the electrochemically synthesized material at different magnifications. Figure 1a shows that ECBBN sorbent consists of aggregates below $40 \mu\text{m}$, and it exhibits various shapes and sizes. Some of the aggregates are basically polyhedrons with relatively plane facets, and it is hard to distinguish the particular aggregates. However, there is also a significant part of the surface, which

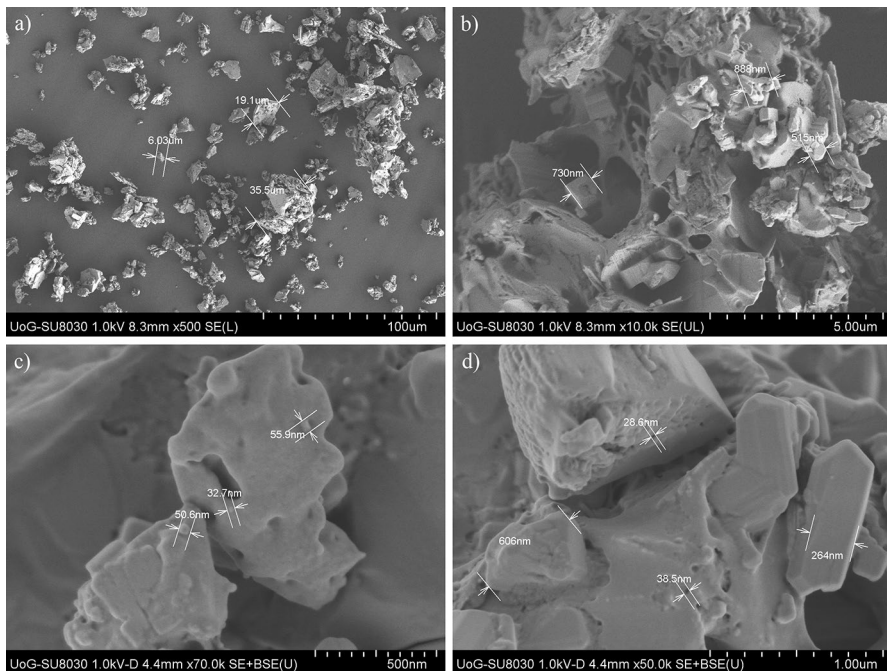


Fig. 1 SEM images of ECBBN at a magnifications of **a** $\times 500$, **b** $\times 10,000$, **c** $\times 70,000$ and **d** $\times 50,000$

appears to be monolithic. Aggregates have porous morphology (Fig. 1b), composed of crystals which are smooth in texture and have a variety of forms. Many of them seem to be sintered, forming much bigger structures. A certain part of the crystals has an irregular structure with plane surface structures which thickness varies between 200 and 800 nm. In Fig. 1c, nanometric crystals with diameter 30–50 nm can be observed. Also, pores smaller than 40 nm in diameter can be detected (Fig. 1d).

Textural properties

The textural properties of ECBBN sorbent have been studied by the nitrogen adsorption measurements. The nitrogen adsorption/desorption isotherms of ECBBN are shown in Fig. 2. According to IUPAC classification, they belong to the isotherm type II, with a type H3 hysteresis loop in the relative pressure range of 0.9–1.0. Such shape of isotherm indicates unrestricted monolayer adsorption on nonporous or macroporous adsorbents. Hysteresis loop of H3 type is characteristic of non-rigid aggregates of plate-like particles and materials, whose pore network consists of macropores [37]. The BET specific surface area of ECBBN is $0.95 \text{ m}^2 \text{ g}^{-1}$. The BJH analysis shows narrow pores with an average pore diameter of 9.99 nm. The mesopore surface area of ECBBN amounts to $0.69 \text{ m}^2 \text{ g}^{-1}$, while the volume of pores is $0.0017 \text{ cm}^3 \text{ g}^{-1}$.

XRD analysis

The XRD spectrum of the synthesized ECBBN is presented in Fig. 3. It shows diffraction peaks at 11.64° , 12.96° , 20.22° , 23.47° , 27.06° , 34.07° , 41.24° and 52.54° 2θ values, which can be indexed to $[\text{Bi}_6\text{O}_5(\text{OH})_3](\text{NO}_3)_5 \cdot 2\text{H}_2\text{O}$ according to the

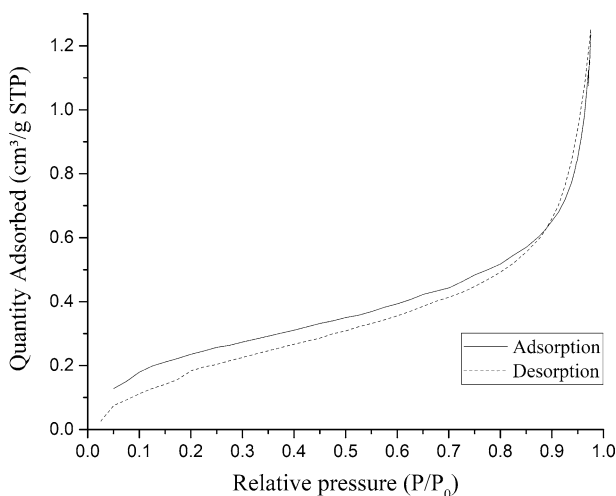


Fig. 2 The N_2 adsorption/desorption isotherm of ECBBN

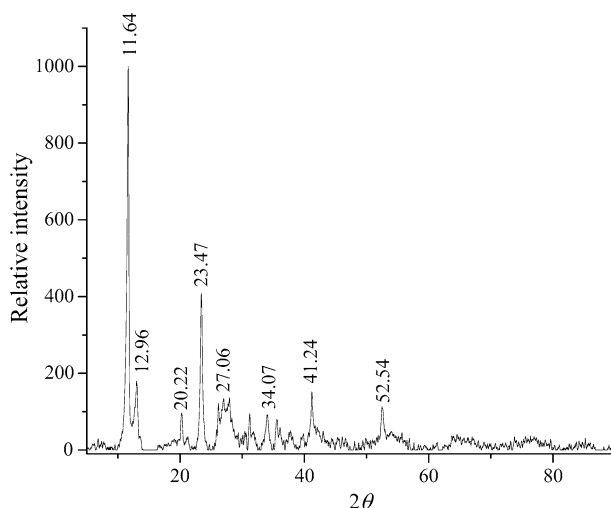


Fig. 3 XRD pattern of ECBBN

XRD database JCPDS-ICDD: PDF-2 00-054-0627. The obtained material is composed of trigonal $[\text{Bi}_6\text{O}_5(\text{OH})_3](\text{NO}_3)_5 \cdot 2\text{H}_2\text{O}$ (space group P-3, $a=b=15.187 \text{ \AA}$, $c=15.838 \text{ \AA}$, $\alpha=\beta=90^\circ$, $\gamma=120^\circ$). Sharp peaks indicate that the synthesized $[\text{Bi}_6\text{O}_5(\text{OH})_3](\text{NO}_3)_5 \cdot 2\text{H}_2\text{O}$ displays high crystallinity. No other phases were found. By using the Williamson–Hall method [38], it is estimated that the crystallite size of the material is $11.3 \pm 0.2 \text{ nm}$.

EDX analysis

EDX analysis (Fig. 4) of electrochemically synthesized material shows the presence of Bi, O and N, which corresponds to typical BBN composition. The weight percentage of elements for ECBBN determined by EDX analysis are given in Table 1, and the results are in good agreement with the theoretical weight percentages for $[\text{Bi}_6\text{O}_5(\text{OH})_3](\text{NO}_3)_5 \cdot 2\text{H}_2\text{O}$.

FTIR analysis

The FTIR spectral analysis is important to identify the characteristic functional groups of material. Figure 5 shows the FTIR spectra of ECBBN sorbent. The broad absorption peak centred at 3421 cm^{-1} is assigned to the stretching vibrations of $-\text{OH}$ groups [39]. The $-\text{OH}$ bending vibration mode of lattice water corresponds to the band at 1626 cm^{-1} [40, 41]. The bands appearing at 718, 811, 1036, 1327, 1354 and 1384 cm^{-1} originate from the NO_3^- vibrations and fit well to the data from the literature [42–44]. The absence of IR bands at 736, 803 and 1297 cm^{-1} is characteristic for hydrated nitrates [43]. Thus, synthesized ECBBN contains water molecules in its structure. The bands observed at 563 and 442 cm^{-1} are assigned to the Bi–O bond stretching vibrations [45, 46]. The FTIR spectrum obtained for the ECBBN

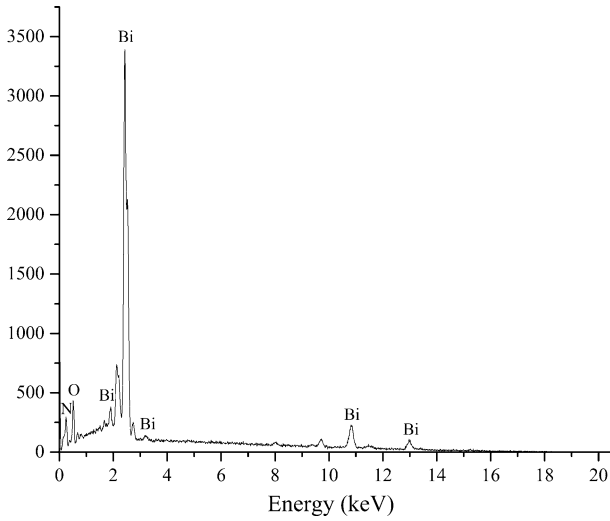


Fig. 4 EDX spectrum of ECBBN

Table 1 Weight percentages of elements in ECBBN by EDX analysis

Element	Experimental weight percentage (%) of elements in ECBBN	Theoretical weight percentage (%) of elements in $[\text{Bi}_6\text{O}_5(\text{OH})_3](\text{NO}_3)_5 \cdot 2\text{H}_2\text{O}$
Bi	73.26	72.43
O	20.73	23.11
N	6.01	4.04
H	–	0.41

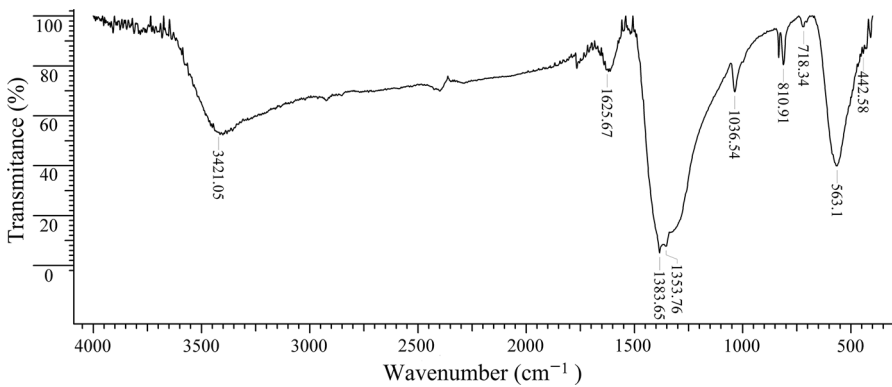


Fig. 5 FTIR spectrum of ECBBN

corresponds to the spectrum of $[\text{Bi}_6\text{O}_5(\text{OH})_3](\text{NO}_3)_5 \cdot 2\text{H}_2\text{O}$ reported by Christensen et al. [47].

The isoelectric point

The isoelectric point (pI) of the synthesized ECBBN sorbent determined by the salt addition method is 2.12, which shows that the sorbent is strongly acidic. The sorbent surface is positively charged at $\text{pH} < 2.12$ and negatively charged at $\text{pH} > 2.12$.

The ability of ECBBN to remove RB19

The ability of the sorbent ECBBN to remove RB19 was studied as a function of time, using an initial sorbent dose of 500.0 mg dm^{-3} , initial RB19 concentration of 500.0 mg dm^{-3} and at native pH. The results (Fig. 6) show that the sorption process occurs in two phases. In the first, initial phase, rapid uptake of RB19 molecules occurs, and during this phase (1 min), more than 95% of the total amount of sorbed dye was removed. The second phase is much slower, and the amount of sorbed dye was less than 5% of the total sorbed amount. From these results, it can be concluded that equilibrium was reached in several minutes, and the maximum amount of sorbed dye at native pH was 838.56 mg g^{-1} . Electrochemically synthesized sorbent (ECBBN) exhibits much higher sorption capacity for RB19 than other sorbents, especially than inorganic sorbents synthesized by conventional methods, such as precipitation, coprecipitation and hydrothermal methods, reported in previous studies (Table 2) [20–27]. Another advantage of the electrochemically synthesized sorbent is much lower sorption equilibrium time, which makes the sorption process considerably faster. Also, ECBBN has substantially higher sorption ability

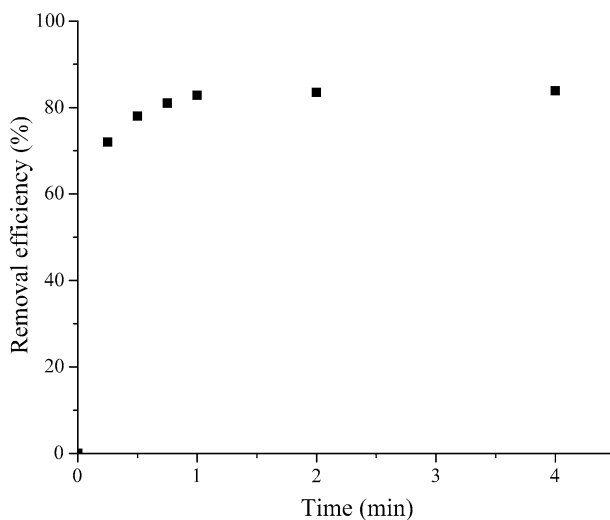
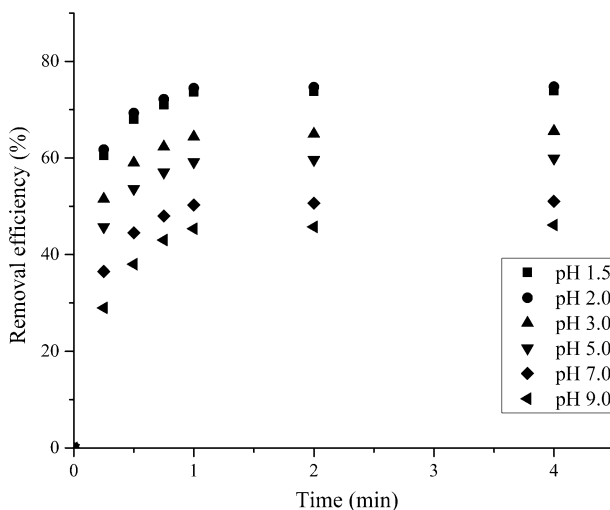


Fig. 6 Effect of contact time on the removal efficiency of RB19. $c_{\text{RB19}} 500.0 \text{ mg dm}^{-3}$, $c_{\text{sorbent}} 500.0 \text{ mg dm}^{-3}$, temperature $25.0 \pm 0.5 \text{ }^\circ\text{C}$, pH native

Table 2 Comparison of sorption capacity of different sorbents for the removal of RB19

Sorbent	Synthesis method	pH	Sorption capacity (mg g ⁻¹)	Equilibrium time (min)	Reference
Magnetite/graphene oxide	Coprecipitation	3.0	62.50	67	[21]
Nanohydroxyapatite	Precipitation	3.0	90.09	180	[20]
NiO nanoparticles	Precipitation	6.5	98.83	15	[22]
Polypyrrole-coated Fe ₃ O ₄	Coprecipitation	3.0	112.36	10	[26]
MgO nanostructures	Hydrothermal	7.8	250.00	20	[23]
Chitosan hollow fibres	–	3.5	454.50	90	[25]
FeCuNi-280	Coprecipitation	2.0	480.80	120	[27]
Chitosan	–	6.8	822.40	150	[24]
ECBBN	Electrochemical	Native pH	838.56	2	This study
ECBBN	Electrochemical	2.0	1046.24	2	This study

**Fig. 7** Effect of pH on the removal efficiency of RB19; c_{RB19} 700.0 mg dm⁻³, c_{sorbent} 500.0 mg dm⁻³, temperature 25.0 ± 0.5 °C

in comparison with BBN reported by Abdullah et al. [31] which is synthesized with precipitation method and has a sorption capacity of 31 and 24 mg g⁻¹ for Methyl Orange and Sunset Yellow, respectively.

Effect of pH on the removal efficiency of RB19

The solution pH is another important parameter in sorption controlling because it affects the surface charge of the sorbent and the degree of ionization of the adsorbate [48]. The effect of pH on the removal efficiency of RB19 was evaluated by changing

the pH from 1.5 to 9.0. All the experiments were carried out with extremely high concentration of RB19 (700 mg dm^{-3}) in order to make it easier to see the difference in the removal efficiency of RB19 at different pH values. From the data in Fig. 7, it can be seen that the maximum removal efficiency of RB19 is achieved at pH 1.5 and 2.0, and it decreases with increasing pH. The removal efficiency decreases from 77.73 to 46.11%, from pH 2.0 to pH 9.0. At pH 1.5, removal efficiency of ECBBN sorbent is slightly lower than at pH 2.0; therefore, experiments were not conducted at pH values lower than 1.5. Under high acidic conditions (pH 1.5–2.0), the surface of the sorbent is positively charged, because the pI of the sorbent is 2.12, and thus the electrostatic attraction between the anionic dye RB19 and the sorbent surface is the strongest at that pH [22]. Therefore, ECBBN has the highest sorption capacity for RB19 at $\text{pH} \leq 2.0$, and it decreases with increasing pH (Fig. 8). The maximum sorption capacity at pH 2.0 is $1046.24 \text{ mg g}^{-1}$. Furthermore, the data in Fig. 8 show that in the whole pH range investigated, i.e. at pH 1.5, 2.0, 3.0, 5.0, 7.0 and 9.0, the sorption capacity is high, being 1034.63, 1046.24, 917.47, 838.56, 714.22 and 645.59 mg g^{-1} , respectively. The minimum sorption capacity is 645.59 mg g^{-1} at pH 9.0, which is still much higher when compared with inorganic sorbents reported in the literature (Table 2). Thus, the high sorption capacity for ECBBN, over the whole investigated pH range, can be considered a beneficial characteristic for the application of the sorbent in water treatment, enabling it to be used without the necessity for pH adjustment and the addition of any other chemical component to the sorption system.

Effect of sorbent dose on the removal efficiency of RB19

The effect of variation in the sorbent dose from 250.0 to $1000.0 \text{ mg dm}^{-3}$ on the removal of RB19 at a constant concentration of RB19 (700.0 mg dm^{-3}) and pH 2 was studied. The removal efficiency of RB19 (Fig. 9) at the lowest dose of sorbent

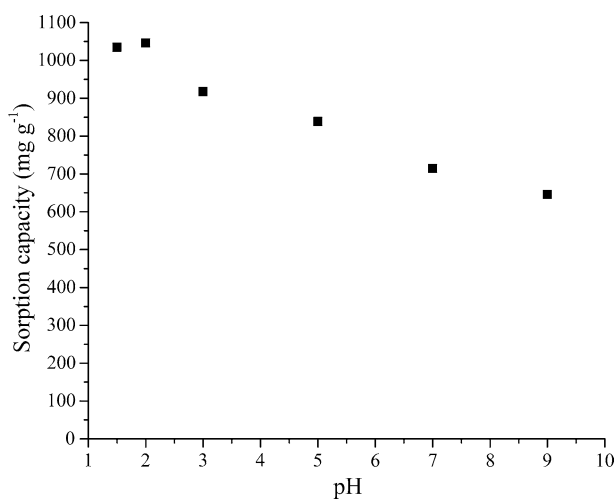


Fig. 8 Sorption capacity of ECBBN at different pH values

(250.0 mg dm⁻³) is low (36.36%). For higher sorbent doses of 500.0, 750.0 and 1000.0 mg dm⁻³, the removal efficiency of RB19 increases up to 74.73, 99.54 and 99.65%, respectively. A rapid increase in the efficiency of dye removal with increasing sorbent dose occurs due to an increase in the surface area of the sorbent and availability of more binding sites for RB19 [8, 49, 50]. Taking into consideration sorption efficiency, sorption amount of dye and the cost of sorbent, a dose of 500.0 mg dm⁻³ of the sorbent is taken as optimum and used for further experiments.

Effect of initial dye concentration on removal efficiency of RB19

Pollutant concentration is one of the most important parameters that can affect the adsorption process. The effect of the initial dye concentration on the removal efficiency was investigated by varying the concentration of RB19 from 100.0 to 700.0 mg dm⁻³ at constant sorbent dose (500.0 mg dm⁻³) and pH 2. The results are presented in Fig. 10, and they show that the removal efficiency decreases from 99.65 to 74.73% with increasing initial concentration of dye from 100.0 to 700.0 mg dm⁻³. The decrease in removal efficiency with increasing dye concentration occurs due to the saturation of the limited available binding sites when using a constant sorbent dose [51].

Kinetics study

Sorption kinetics study is very important for a complete understanding of the sorption behaviour. To evaluate the sorption mechanisms and identify the potential rate-controlling steps, reaction and diffusion kinetic models were used to test the

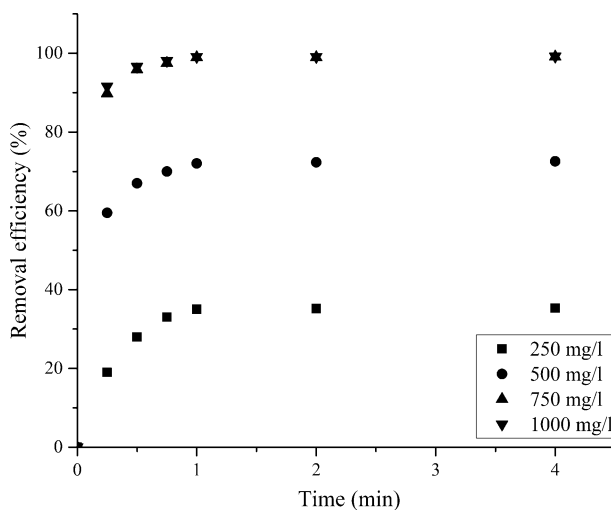


Fig. 9 Effect of sorbent dose on the removal efficiency of RB19. c_{RB19} 700.0 mg dm⁻³, temperature 25.0 ± 0.5 °C, pH 2.0

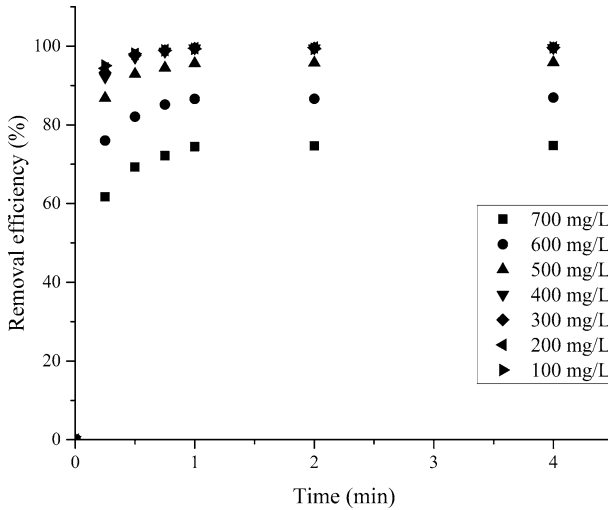


Fig. 10 Effect of initial concentration of dye on the removal efficiency of RB19; $c_{\text{sorbent}} 500.0 \text{ mg dm}^{-3}$, temperature $25.0 \pm 0.5 \text{ }^\circ\text{C}$, pH 2.0

experimental data. Pseudo-first-order and pseudo-second-order reaction kinetics models nonlinear form of equations are expressed as follows:

$$q_t = q_e(1 - e^{-k_1 t}) \quad (4)$$

$$q_t = \frac{q_e^2 k_2 t}{1 + k_2 q_e t} \quad (5)$$

where q_t is amount of dye sorbed at time t (mg g^{-1}), q_e (mg g^{-1}) is amount of dye sorbed at equilibrium state, k_1 (min^{-1}) and k_2 ($\text{g mg}^{-1} \text{ min}^{-1}$) are pseudo-first and pseudo-second-order reaction rate constants, respectively [52, 53].

The intraparticle diffusion model proposed by Weber and Morris was used for the description of the diffusion mechanism, and it is expressed by the following equation:

$$q_t = k_{\text{id}} t^{1/2} + C \quad (6)$$

where k_{id} ($\text{mg g}^{-1} \text{ min}^{-1/2}$) is the intraparticle diffusion rate constant, q_t (mg g^{-1}) is the amount of RB19 sorbed at time t and C is the constant varied directly with the boundary layer thickness [54].

All the parameters, which characterize these models, were determined by nonlinear regression analysis of experimental data for pseudo-first-order and pseudo-second-order models and linear for the intraparticle diffusion model. Regression analysis was done using software OriginPro 2016, and results are presented in Table 3.

The determination coefficients for both reactions kinetic models are higher than 0.999, which indicates that both models can be successfully applied for the sorption process. Similar values of the calculated q_e with experimentally determined $q_{e, \text{exp}}$

Table 3 Kinetic parameters for RB19 sorption onto ECBBN sorbent

c (mg dm ⁻³)	100	200	300	400	500	600	700
$q_{e, \text{exp}}$ (mg g ⁻¹)	199.32	398.63	597.27	796.58	959.02	1043.00	1046.24
Pseudo-first-order model							
q_e (mg g ⁻¹)	197.92	396.48	593.93	790.82	949.59	1027.01	1028.02
k_1 (min ⁻¹)	12.88	12.09	11.35	10.65	9.71	8.53	7.09
r^2	0.9999	0.9998	0.9998	0.9996	0.9995	0.9986	0.9981
RMD (%)	0.30	0.39	0.44	0.57	0.71	1.20	1.63
Pseudo-second-order model							
q_e (mg g ⁻¹)	200.96	403.95	607.22	811.93	981.47	1074.13	1093.96
k_2 (g mg ⁻¹ min ⁻¹)	0.36	0.15	0.08	0.05	0.03	0.02	0.01
r^2	0.9999	0.9999	0.9999	0.9998	0.9997	0.9996	0.9993
RMD (%)	0.27	0.28	0.37	0.44	0.53	0.65	0.76
Intraparticle diffusion model							
k_{i1} (mg g ⁻¹ min ^{-1/2})	296.40	591.45	882.33	1168.17	1391.82	1472.57	1437.58
C_1 (mg g ⁻¹)	9.50	18.53	26.88	34.66	39.01	39.79	32.90
r^2	0.9060	0.9115	0.9181	0.9140	0.9259	0.9229	0.9393
k_{i2} (mg g ⁻¹ min ^{-1/2})	1.06	1.80	2.70	4.61	9.12	13.50	22.62
C_2 (mg g ⁻¹)	197.20	395.43	592.50	788.26	942.45	1018.06	1005.96
r^2	0.9207	0.9297	0.9297	0.9388	0.9223	0.9301	0.9381

also confirms the applicability of these kinetic models. The obtained q_e values for the pseudo-first-order model are in slightly better agreement with experimental data in comparison with results obtained for the pseudo-second-order model. However, for all tested concentrations lower RMD values for the pseudo-second-order than for the pseudo-first-order model were obtained, which indicates that pseudo-second-order model fitted the experimental data slightly better. Thus, obtained results suggest that the rate-controlling step in the sorption process might be surface reaction through electron sharing/exchange between RB19 and active sites of sorbent, ion exchange reaction, complexation, coordination and/or chelation [55, 56]. A small specific surface area of the sorbent also indicates that the above-mentioned processes have a greater impact on the sorption process than the physical sorption. The values of pseudo-second-order reaction rate constants, k_2 , decrease with increasing initial RB19 concentration, because almost all available binding sites at the sorbent surface are free at lower initial dye concentrations, resulting in high reaction rate constant values. With higher dye concentrations, saturation of binding sites occurs, which leads to a decrease of the k_2 values.

The results of linear regression analysis for the intraparticle diffusion model are given in Table 3. The two linear ranges in the shape of the intraparticle diffusion plot of q_t versus $t^{1/2}$ indicate that two steps occur in the adsorption process. The first, sharp linear range can be ascribed to the external surface adsorption or instantaneous adsorption stage of RB19 on the sorbent. When the adsorption onto the external surface reaches saturation, the second linear range begins, which represents the gradual adsorption stage, where the intraparticle diffusion is rate-controlled [57].

The first step is very fast, finished in about 1 min, while the second step is very slow, and after the first minute, the change of amount of sorbed dye is negligible. The intraparticle diffusion rate constant k_{i2} is much lower than k_{i1} , which confirms that the rate-limiting step is intraparticle diffusion through the boundary layer.

The results which show that both reaction models have very good agreement with experimental data and that the intraparticle model shows that the sorption process ends quickly (very small slope of the second linear part which starts after 1 min) prove enormous rate of sorption process with mixed control by surface reactions and diffusion.

Adsorption isotherms

The isotherm models were used for investigation of adsorption equilibrium between the ECBBN sorbent and textile dye RB19. Adsorption isotherms measurements were carried out by varying the RB19 concentration between 100.0 and 700.0 mg dm⁻³ at pH 2.0. Several adsorption isotherms, such as Langmuir [58], Freundlich [59], Redlich–Peterson [60] and Brouers–Sotolongo [61, 62], were applied to simulate the experimental data. Langmuir model assumes monolayer adsorption at specific homogeneous surfaces on uniformly energetic adsorption sites, with no lateral interaction between adsorbed molecules. Freundlich model was applied to multilayer adsorption at a heterogeneous surface with non-uniform distribution of adsorption heat and affinities over the heterogeneous surface. The Redlich–Peterson isotherm is a combined form of Langmuir and Freundlich equations and assumes that adsorption does not follow ideal monolayer adsorption. Brouers–Sotolongo isotherm model predicts adsorption at the heterogeneous surface. These adsorption isotherms can be expressed in a nonlinear form by the following equations:

$$q_e = \frac{q_m K_L c_e}{1 + K_L c_e} \quad (7)$$

$$q_e = K_F c_e^n \quad (8)$$

$$q_e = \frac{K_{RP} c_e}{1 + \alpha_{RP} c_e^\beta} \quad (9)$$

$$q_e = q_m (1 - \exp(-K_W c_e^\alpha)) \quad (10)$$

where q_e (mg g⁻¹) is the amount of RB19 sorbed by the sorbent at equilibrium time; c_e (mg dm⁻³) is the concentration of RB19 at equilibrium time in solution; q_m (mg g⁻¹) is the maximum sorption capacity of sorbent; K_L (dm³ mg⁻¹) is Langmuir constant related to the energy of sorption, K_F ((mg g⁻¹) (dm³ mg⁻¹)^{1/n}) is Freundlich equilibrium constant, n is Freundlich exponent related to the intensity of sorption, K_{RP} (dm³ g⁻¹) is the Redlich–Peterson isotherm constant, α_{RP} is also a constant having unit of dm³ mg⁻¹, β is an exponent varied between 0 and 1, K_W (dm³ mg⁻¹) is

Brouers–Sotolongo isotherm constant and the dimensionless exponent α is a measure of the width of the sorption energy distribution and therefore of the energy heterogeneity of the surface.

These isotherms were characterized by parameters, which express affinity and surface properties of sorbents. All parameters of these isotherms models were determined by nonlinear regression analysis using OriginPro 2016, and the results are given in Table 4.

Applicability of these models was determined by determination coefficients and relative mean deviations. The Langmuir, Redlich–Peterson and Brouers–Sotolongo sorption isotherms have very high r^2 values (higher than 0.98), while the Freundlich model has significantly lower determination coefficient (0.72) than these three models. In addition, RMD for the Freundlich model (16.57%) is the highest, which confirms that the sorption process does not follow the Freundlich isotherm. The other three models have much lower values of RMD , 3.14%, 3.19% and 3.85% for Langmuir, Redlich–Peterson and Brouers–Sotolongo, respectively. The obtained q_m for Langmuir model (1049.19 mg g⁻¹) is in slightly better agreement with experimental data (1046.24 mg g⁻¹) in comparison with q_m for Brouers–Sotolongo model (1014.86 mg g⁻¹). Based on r^2 , RMD and results for maximum sorption capacity, it can be concluded that among of all above-mentioned models Langmuir, Redlich–Peterson and Brouers–Sotolongo models can be used to describe sorption of RB19 on ECBBN sorbent, and for the nuance, Langmuir model has better matching with experimental results than the other models. The Redlich–Peterson exponent β is close to 1, and for that value these isotherm model is effectively reduced to the Langmuir model, which means that Langmuir will be preferable isotherm in comparison with Freundlich. Brouers–Sotolongo exponent α , which is in relation with the heterogeneity of the surface, is also close to 1 and indicates that adsorption sites of ECBBN sorbent are homogenous. Based on the applied isotherm models, it can be inferred that the sorption has homogenous character, which confirms good agreement with the Langmuir type of isotherm.

R_L is a dimensionless constant (commonly known as separation factor) derived from the Langmuir isotherm, which can be expressed as follows [63]:

Table 4 Isotherm parameters for RB19 sorption onto ECBBN sorbent

Adsorption isotherm	Parameter	Values	r^2	RMD (%)
Langmuir	K_L	0.91	0.9895	3.14
	q_m	1049.19		
Freundlich	K_F	515.14	0.7596	16.57
	n	6.37		
Redlich–Peterson	K_{RP}	929.68	0.9872	3.19
	α_{RP}	0.86		
	β	1.01		
Brouers–Sotolongo	K_W	0.65	0.9851	3.85
	q_m	1014.86		
	α	0.93		

$$R_L = \frac{1}{1 + K_L c_0} \quad (11)$$

It describes the adsorption nature, which can be defined as unfavourable ($R_L > 1$), linear ($R_L = 1$), favourable ($0 < R_L < 1$) or irreversible ($R_L = 0$). The R_L values were found to be from 0.0108 to 0.0016 as the initial concentration of dye increases from 100 to 700 mg dm⁻³. This means that the reaction is more favourable for high RB19 concentrations. The value of Freundlich exponent ($1/n < 1$) confirms that adsorption is favourable.

The mechanism of sorption of RB19 onto ECBBN sorbent

According to all the results described in the manuscript, it can be concluded that the mechanism of RB19 sorption on ECBBN sorbent is complex, and the possible mechanism can be presented as follows. From the results of the influence of pH, it can be seen that the sorption capacity is the highest at pH 2 and it continually decreases with increasing pH to 9. However, at pH 9, the sorption capacity is still very high. Thus, it is obvious that electrostatic interactions, which mainly occur at low pH values, are not the only mechanism of the sorption process: the complexation also affects the sorption process. Since sulphonic acids are very strong acids (their pK_a values are low), sulphonic groups of the RB19 dye will be dissociated ($-\text{SO}_3^-$) in the entire investigated range of pH. So, chemical interaction of sulphonic group of RB19 with polycation $[\text{Bi}_6\text{O}_5(\text{OH})_3]^{5+}$ of ECBBN occurs in the whole range of pH. In contrast, the contribution of physical sorption is small due to the small specific surface area of ECBBN, and therefore, mechanism of the sorption process is the most likely combination of electrostatic and chemical interactions between RB19 and ECBBN sorbent.

Treatment of a model solution of polluted Nišava River water

In order to investigate the applicability of ECBBN in the purification of real polluted water, treatment of a model solution of river water contaminated with RB19 was done. The river water samples were collected from Nišava River and were used without further treatment, except the filtration through 0.45 μm regenerated cellulose membrane filter. The river water was used as the matrix of the solutions used in the experiments. A model solution of polluted river water was made by adding 500.0 mg dm³ of RB19 to the matrix. According to the previous results, experiments were done at optimal conditions by using a sorbent dose of 500.0 mg dm³ and at pH 2.0. Results (Fig. 11) show that the removal efficiency of RB19 from model solution of contaminated river water is also high, but the sorption capacity, as expected, is slightly lower than in model solution made with deionized water. Sorption capacity in the model solution of polluted river water was 838.25 mg dm³, which is 19.88% lower in comparison with the deionized water model solution. This may be attributed to the presence of organic matter in the river water, which can be also sorbed

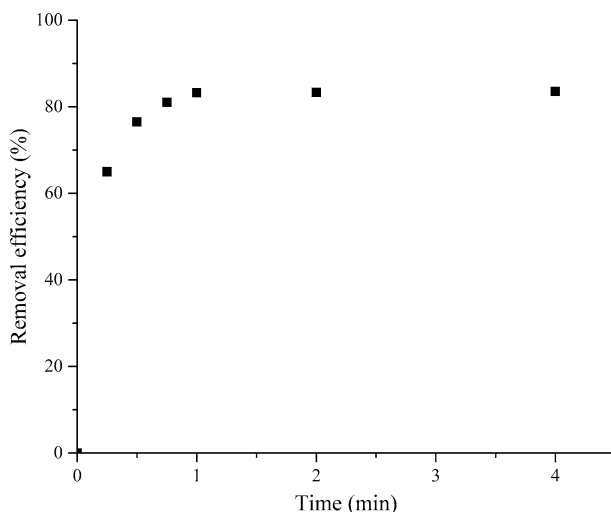


Fig. 11 Effect of contact time on the removal efficiency of RB19 in the model solution of polluted river water. $c_{\text{RB19}} 500.0 \text{ mg dm}^{-3}$, $c_{\text{sorbent}} 500.0 \text{ mg dm}^{-3}$, temperature $25.0 \pm 0.5 \text{ }^\circ\text{C}$, pH 2.0

at the active sites of ECBBN sorbent. The high sorption capacity of ECBBN for the removal of RB19 from the river water indicates that this material can be suitable sorbent for the textile dyes removal from real polluted water.

Conclusions

Pure basic bismuth nitrate $[\text{Bi}_6\text{O}_5(\text{OH})_3](\text{NO}_3)_5 \cdot 2\text{H}_2\text{O}$ was, for the first time, successfully synthesized by electrochemical deposition, followed by thermal treatment at $200 \text{ }^\circ\text{C}$. The chemical structure of ECBBN was ascertained by XRD, FTIR and EDX analyses. The material is composed of small crystals forming high aggregates; the crystallite size is $11.3 \pm 0.2 \text{ nm}$. Sorption of RB19 by electrochemically synthesized sorbent (ECBBN) is very fast (above 95% of the total sorption at equilibrium was reached in 1 min). Sorption kinetics shows that both surface reaction and diffusion were rate-limiting steps. Based on the determination coefficients and relative mean deviations it can be deduced that the experimental data were the best fitted with Langmuir isotherm. The maximum sorption capacity ($1049.19 \text{ mg g}^{-1}$) was achieved at pH 2.0. Very high sorption capacity and fast equilibration are very important characteristics for the potential practical use of ECBBN, as well as high sorption capacity in model solutions of contaminated river water. The removal efficiency of RB19 increases with increasing sorbent dose and decreasing dye concentration. Low cost, eco-friendly starting materials, simple and non-time consuming synthesis method, high purity and repeatability of the synthesized material structure, as well as very high sorption capacity, better sorption performance and lower

sorption equilibrium time than similar materials, make ECBBN sorbent a very attractive system for the removal of textile dyes from polluted water.

Acknowledgements The authors would like to acknowledge financial support from the Ministry of Education, Science and Technological Development of the Republic of Serbia (Grant No. TR34008).

References

1. D. Brown, H.R. Hitz, L. Schäfer, *Chemosphere* **10**, 245 (1981)
2. S. Padmavathy, S. Sandhya, K. Swaminathan, Y.V. Subrahmanyam, T. Chakrabarti, S.N. Kaul, *Chem. Biochem. Eng. Q.* **17**, 147 (2003)
3. L. Ćurković, D. Ljubas, H. Juretić, *React. Kinet. Mech. Catal.* **99**, 201 (2009)
4. S. Peng, D. Zhang, H. Huang, Z. Jin, X. Peng, *Res. Chem. Intermed.* **45**, 1545 (2019)
5. T. Robinson, G. McMullan, R. Marchant, P. Nigam, *Bioresour. Technol.* **77**, 247 (2001)
6. J. Pierce, *J. Soc. Dye. Colour.* **110**, 131 (1994)
7. Y.L. Qi, Y.F. Zheng, X.C. Song, *J. Taiwan Inst. Chem. Eng.* **71**, 355 (2017)
8. G. Moussavi, M. Mahmoudi, *J. Hazard. Mater.* **168**, 806 (2009)
9. S. Banerjee, G.C. Sharma, R.K. Gautam, M.C. Chattopadhyaya, S.N. Upadhyay, Y.C. Sharma, *J. Mol. Liq.* **213**, 162 (2016)
10. J. Fan, D. Yu, W. Wang, B. Liu, *Cellulose* **26**, 3955 (2019)
11. K. Ding, W. Wang, D. Yu, W. Wang, P. Gao, B. Liu, *Appl. Surf. Sci.* **454**, 101 (2018)
12. Y. Huang, Z. Guo, H. Liu, S. Zhang, P. Wang, J. Lu, and Y. Tong, *Adv. Funct. Mater.* (2019). <https://doi.org/10.1002/adfm.201903490>
13. K. Ye, Y. Li, H. Yang, M. Li, Y. Huang, S. Zhang, H. Ji, *Appl. Catal. B Environ.* **259**, 118085 (2019)
14. Y. Wang, D. Yu, W. Wang, P. Gao, L. Zhang, S. Zhong, B. Liu, *Coll. Surf. A Physicochem. Eng. Asp.* **578**, 123608 (2019)
15. K. Ding, D. Yu, W. Wang, P. Gao, B. Liu, *Appl. Surf. Sci.* **445**, 39 (2018)
16. L. Lin, D. Yu, W. Wang, P. Gao, K. Bu, B. Liu, *Mater. Lett.* **185**, 507 (2016)
17. B. Liu, L. Lin, D. Yu, J. Sun, Z. Zhu, P. Gao, W. Wang, *Cellulose* **25**, 1089 (2018)
18. R. Yang, F. Dong, X. You, M. Liu, S. Zhong, L. Zhang, B. Liu, *Mater. Lett.* **252**, 272 (2019)
19. Z. Zhu, Q. Han, D. Yu, J. Sun, B. Liu, *Mater. Lett.* **209**, 379 (2017)
20. G. Ciobanu, S. Barna, M. Harja, *Arch. Environ. Prot.* **42**, 3 (2016)
21. Z. Ayazi, Z.M. Khoshhesab, S. Norouzi, *Desalin. Water Treat.* **57**, 25301 (2016)
22. Z.M. Khoshhesab, M. Ahmadi, *Desalin. Water Treat.* **57**, 20037 (2015)
23. N.K. Nga, P.T.T. Hong, T.D. Lam, T.Q. Huy, *J. Colloid Interface Sci.* **398**, 210 (2013)
24. N.K. Nga, H.D. Chinh, P.T.T. Hong, T.Q. Huy, *J. Polym. Environ.* **25**, 146 (2016)
25. A. Mirmohseni, M.S. Seyed Dorraji, A. Figoli, F. Tasselli, *Bioresour. Technol.* **121**, 212 (2012)
26. M. Shanehsaz, S. Seidi, Y. Ghorbani, S.M.R. Shoja, S. Rouhani, *Spectrochim. Acta Part A Mol. Biomol. Spectrosc.* **149**, 481 (2015)
27. M. Kostić, M. Radović, N. Velinov, S. Najdanović, D. Bojić, A. Hurt, A. Bojić, *Ecotoxicol. Environ. Saf.* **159**, 332 (2018)
28. Y. Yang, H. Liang, N. Zhu, Y. Zhao, C. Guo, L. Liu, *Chemosphere* **93**, 701 (2013)
29. L. Xie, J. Wang, Y. Hu, Z. Zheng, S. Weng, P. Liu, X. Shi, D. Wang, *Mater. Chem. Phys.* **136**, 309 (2012)
30. Y. He, Y. Zhang, H. Huang, N. Tian, Y. Luo, *Inorg. Chem. Commun.* **40**, 55 (2014)
31. E.A. Abdullah, A.H. Abdullah, Z. Zainal, M.Z. Hussein, T.K. Ban, *E-J. Chem.* **9**, 1885 (2012)
32. Y.M. Yukhin, T.V. Daminova, L.I. Afonina, B.B. Bokhonov, O.A. Logutenko, A.I. Aparnev, K.Y. Mikhailov, T.A. Udalovala, V.I. Evseenko, *Chem. Sustain. Dev.* **12**, 395 (2004)
33. I. Zhitomirsky, *Adv. Colloid Interface Sci.* **97**, 279 (2002)
34. S. Brunauer, P.H. Emmett, E. Teller, *J. Am. Chem. Soc.* **60**, 309 (1938)
35. E.P. Barrett, L.G. Joyner, P.P. Halenda, *J. Am. Chem. Soc.* **73**, 373 (1951)

36. T. Mahmood, M.T. Saddique, A. Naeem, P. Westerhoff, S. Mustafa, A. Alum, *Ind. Eng. Chem. Res.* **50**, 10017 (2011)
37. M. Thommes, K. Kaneko, A.V. Neimark, J.P. Olivier, F. Rodriguez-Reinoso, J. Rouquerol, K.S.W. Sing, *Pure Appl. Chem.* **87**, 1051 (2015)
38. G. Williamson, W. Hall, *Acta Metall.* **1**, 22 (1953)
39. X.-D. Liu, H. Masato, X.-G. Zheng, W.-J. Tao, D.-D. Meng, S.-L. Zhang, Q.-X. Guo, *Chin. Phys. Lett.* **28**, 017803 (2011)
40. Z. Ding, G.Q. Lu, P.F. Greenfield, *J. Phys. Chem. B* **104**, 4815 (2000)
41. T. Wajima, Y. Umeta, S. Narita, K. Sugawara, *Desalination* **249**, 323 (2009)
42. P. Ziegler, I. Grigoraviciute, K. Gibson, J. Glaser, A. Kareiva, H.J. Meyer, *J. Solid State Chem.* **177**, 3610 (2004)
43. W.T. Carnall, S. Siegel, J.R. Ferraro, B. Tani, E. Gebert, *Inorg. Chem.* **12**, 560 (1973)
44. J.-C.G. Bünzli, E. Moret, J.-R. Yersin, *Helv. Chim. Acta* **61**, 762 (1978)
45. R. Irmawati, M.N.N. Nasriah, Y.H. Taufiq-Yap, S.B.A. Hamid, *Catal. Today* **93–95**, 701 (2004)
46. V. Fruth, M. Popa, D. Berger, C.M. Ionica, M. Jitianu, *J. Eur. Ceram. Soc.* **24**, 1295 (2004)
47. A.N. Christensen, M. Chevallier, J. Skibsted, B.B. Iversen, *J. Chem. Soc., Dalton Trans.* 265 (2000)
48. V. Kumari, A. Bhamik, *Dalton Trans.* **44**, 11843 (2015)
49. H. Javadian, M.T. Angaji, M. Naushad, *J. Ind. Eng. Chem.* **20**, 3890 (2014)
50. S. Li, J. Zhang, S. Jamil, Q. Cai, S. Zang, *Res. Chem. Intermed.* **44**, 3933 (2018)
51. M.A. Behnajady, S. Yavari, N. Modirshahla, *Chem. Ind. Chem. Eng. Q.* **20**, 97 (2014)
52. Y.S. Ho, G. McKay, *Chem. Eng. J.* **70**, 115 (1998)
53. S. Lagergren, K. Sven, *Vetenskapsakademiens Handl.* **24**, 1 (1898)
54. W.J. Weber, J.C. Morris, *J. Sanit. Eng. Div.* **89**, 31 (1963)
55. Y.F. Lam, L.Y. Lee, S.J. Chua, S.S. Lim, S. Gan, *Ecotoxicol. Environ. Saf.* **127**, 61 (2016)
56. T. Todorciuc, L. Bulgariu, V.I. Popa, *Cellul. Chem. Technol.* **49**, 439 (2015)
57. K. Vijayaraghavan, J. Mao, Y.S. Yun, *Bioresour. Technol.* **99**, 2864 (2008)
58. I. Langmuir, *J. Am. Chem. Soc.* **40**, 1361 (1918)
59. H. Freundlich, *Z. Für Phys. Chem.* **57**, 385 (1906)
60. O. Redlich, D.L. Peterson, *J. Phys. Chem.* **63**, 1024 (2007)
61. F. Brouers, O. Sotolongo, F. Marquez, J.P. Pirard, *Phys. A Stat. Mech. Appl.* **349**, 271 (2005)
62. M.C. Ncibi, S. Altener, M. Seffen, F. Brouers, S. Gaspard, *Chem. Eng. J.* **145**, 196 (2008)
63. K.R. Hall, L.C. Eagleton, A. Acrivos, T. Vermeulen, *Ind. Eng. Chem. Fundam.* **5**, 212 (1966)

Publisher's Note Springer Nature remains neutral with regard to jurisdictional claims in published maps and institutional affiliations.